

Observation of the Sign Reversal of the Magnetic Correlation in a Driven-Dissipative Fermi-Hubbard System

Kantaro Honda,^{1,*} Shintaro Taie,¹ Yosuke Takasu,¹ Naoki Nishizawa,¹ Masaya Nakagawa,² and Yoshiro Takahashi¹

¹*Department of Physics, Graduate School of Science, Kyoto University, Kyoto 606-8502, Japan*

²*Department of Physics, University of Tokyo, 7-3-1 Hongo, Bunkyo-ku, Tokyo 113-0033, Japan*

(Dated: May 27, 2022)

We report the observation of the sign reversal of the magnetic correlation from antiferromagnetic to ferromagnetic in a dissipative Fermi-Hubbard system, utilizing the dissipation caused by on-site two-body losses in a controlled manner. We systematically measure dynamics of the nearest-neighbor spin correlation in a double-well optical lattice, as well as a crossover of a double-well lattice to a one-dimensional uniform lattice. In a wide range of lattice configurations over a double-well lattice, we observe a ferromagnetic spin correlation, which is interpreted as a transient state leading to a Dicke state. This work demonstrates the control of quantum magnetism in open quantum systems with dissipation.

Dissipation, which is caused by the coupling to the environment, plays a crucial role in quantum systems. On the one hand, it disturbs the coherent dynamics in quantum systems, which is unfavorable for many quantum information processing as well as the study of quantum phases. On the other hand, dissipation can play a novel role in preparing and manipulating quantum states of interest [1, 2]. In cold atom systems, which are often regarded as ideal isolated quantum systems, it is also possible to study open quantum systems by making use of their high controllability. So far, dissipative systems with one [3–8], two- [9–12] and three-body particle losses [13, 14] have been investigated, and part of novel phenomena brought about only by the presence of dissipation has been clarified.

In quantum magnetism, dissipation can also have a great influence on its equilibrium state. In the previous work, sign reversal of magnetic correlations from antiferromagnetic to ferromagnetic in a dissipative system with on-site two-body losses is theoretically predicted [15] (Fig. 1). For a dissipative system, the formation of a highly entangled Dicke state [16], which has a fully symmetric spin wave function, is also predicted [17, 18]. Experimentally, atom loss dynamics in the one-dimensional (1D) dissipative Fermi-Hubbard system has been investigated, and the dynamical generation of the Dicke state has been inferred based on the suppressed atom losses after initial fast transient dynamics [19]. However, in Ref. [19], spin correlations, which are a more direct signature of the ferromagnetism characterizing the Dicke state, have not been directly measured. Moreover, a fixed strength of dissipation was introduced, and therefore systematic study of dissipative dynamics with controllable strength of dissipation was not carried out.

In this Letter, we implement a driven-dissipative Fermi-Hubbard system with on-site two-body losses. Engineered dissipation is introduced in a controlled manner by a photoassociation (PA) process [11] (Fig. 1). This system is described by the dissipative Fermi-Hubbard

model, and the dynamics of its density matrix $\hat{\rho}$ is described by the following quantum master equation [15, 18]:

$$\frac{d\hat{\rho}}{d\tau} = \frac{i}{\hbar}[\hat{\rho}, \hat{H}] + \frac{1}{2} \sum_{j,\sigma \neq \sigma'} \left(\hat{L}_{j\sigma\sigma'} \hat{\rho} \hat{L}_{j\sigma\sigma'}^\dagger - \frac{1}{2} \{ \hat{L}_{j\sigma\sigma'}^\dagger \hat{L}_{j\sigma\sigma'}, \hat{\rho} \} \right), \quad (1)$$

$$\hat{H} = -t \sum_{\langle i,j \rangle, \sigma} \left(\hat{c}_{i\sigma}^\dagger \hat{c}_{j\sigma} + \text{H.c.} \right) + \frac{U}{2} \sum_{j,\sigma \neq \sigma'} \hat{n}_{j\sigma} \hat{n}_{j\sigma'}, \quad (2)$$

where $\hat{c}_{i\sigma}$ is the fermionic annihilation operator for a site i and spin σ , $\hat{n}_{j\sigma} = \hat{c}_{j\sigma}^\dagger \hat{c}_{j\sigma}$ is the number operator, t is the tunneling amplitude between nearest-neighbor sites, U is the on-site interaction strength, and $\hat{L}_{j\sigma\sigma'} = \sqrt{2\gamma} \hat{c}_{j\sigma} \hat{c}_{j\sigma'}$ is the Lindblad operator, which describes the on-site two-body loss with the loss rate γ . In dissipative double-well systems, we systematically measure the dynamics of nearest-neighbor spin correlations. Here, spin correlations are directly measured with a singlet-triplet oscil-

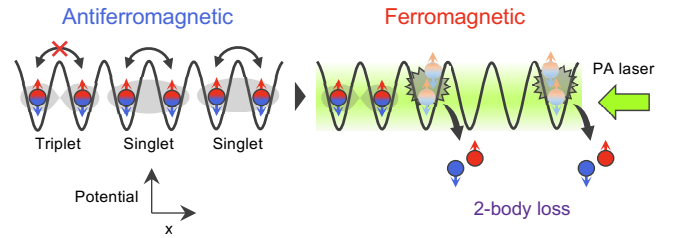


FIG. 1. Schematic illustration of the mechanism of the reversal of the magnetic correlation from the antiferromagnetic (left) to the ferromagnetic correlation (right) in a dissipative system with on-site two-body losses. While double occupancy on the same site occurs in the singlet state, which has a spatially symmetric wave function, it is prohibited by the Pauli exclusion principle in the triplet state, which has a spatially antisymmetric wave function. Thus, only singlet states are lost under on-site two-body losses, which makes the nearest-neighbor magnetic correlation reverse. In this work, we induce on-site two-body losses with a laser utilizing the PA.

lation (STO) [20, 21]. We successfully observe the dynamical sign reversal of magnetic correlations. We also investigate the dependency of the spin correlation dynamics on the dissipation strength and the exchange interaction. These experimental results are in good agreement with the theoretical predictions in Ref. [15]. Moreover, we measure spin correlations in a crossover from a double-well lattice to a 1D uniform lattice, where we observe a sign-reversed magnetic correlation, which more directly suggests the formation of a transient ferromagnetic spin correlation leading to a highly entangled Dicke state. This work demonstrates the control of magnetic correlations and their sign in open quantum systems with dissipation. Note that, in an isolated quantum system, a novel Floquet engineering method [22] was utilized for the manipulation of quantum magnetism [23].

Experimental setup.— A degenerate Fermi gas of six-component ^{173}Yb ($T/T_F \sim 0.15$, T_F : Fermi temperature), which is generated by evaporative cooling, is loaded into an optical superlattice which realizes a dimerized or a 1D optical lattice as well as the crossover between them. Our optical lattice potential is given by

$$V(x, y, z) = -V_{\text{short}}^{(z)} \cos^2(2k_L z + \pi/2) - V_{\text{long}}^{(z)} \cos^2(k_L z) - V_{\text{short}}^{(x)} \cos^2(2k_L x) - V_{\text{short}}^{(y)} \cos^2(2k_L y), \quad (3)$$

where $k_L = 2\pi/\lambda$ with $\lambda = 1064$ nm is the wave number of the long lattice ($V_{\text{long}}^{(z)} = 0$ for a 1D uniform optical lattice). In the following, we represent the potential depth of the optical lattice as $s_L = [s_{\text{short}}^{(x)}, s_{\text{short}}^{(y)}, (s_{\text{short}}^{(z)}, s_{\text{long}}^{(z)})] = [V_{\text{short}}^{(x)}, V_{\text{short}}^{(y)}, (V_{\text{short}}^{(z)}, V_{\text{long}}^{(z)})]/E_R$, where $E_R = \hbar^2 k_L^2/2m$ is the recoil energy for the long lattice. Typical parameters for the optical superlattice are $s_L = [80, 80, (20.8, 20)]$, and the corresponding Hubbard parameters are $t_d/h = 1.0$ kHz, $U/t_d = 4.0$, $t/h = 38$ Hz, and $t_x/h = t_y/h = 10$ Hz, where $t_d, t, t_{x(y)}$ are the tunneling amplitudes between intra-dimer sites, inter-dimer sites along the z -axis and inter-dimer sites along the $x(y)$ -axis, respectively. Here, the tunneling amplitudes along the dimerized lattice are determined by fitting a tight-binding model to the energy bands obtained from the first principle calculation for the superlattice potential. For the on-site interaction strength, we constructed the Wannier function with the method described in Ref. [24].

In this work, we introduce on-site two-body losses as dissipation utilizing PA technique. In the PA process, two ground-state atoms in a doubly occupied site where PA laser is irradiated are converted to an electronically excited short-lived molecule, which rapidly escapes from an optical trap [11, 20, 21, 25]. In this way, on-site two-body losses are realized with PA laser, enabling us to control the dissipation strength by controlling the PA laser intensity. Use of the deep PA resonance, far

detuned by -5.76 GHz from the $^1S_0 \leftrightarrow ^3P_1$ ($F' = 7/2$) transition, is effective to suppress the one-body loss and heating due to photon scattering.

To directly measure nearest-neighbor spin correlations, we utilize a singlet-triplet oscillation (STO) [26] which is optically induced with a spin-dependent potential gradient [see Sec. S.1 in the Supplemental Material (SM) [27] for the details of STO measurement]. A typical STO signal for a six-component mixture in a dimerized lattice is shown in Fig. 2(a) (upper left). This signal form, which has a positive slope at the initial time, reveals an excess number of singlets compared to triplets, corresponding to the antiferromagnetic correlation between nearest-neighbor sites. To quantitatively evaluate the magnetic correlation, we fit the data with an empirical function

$$f(t) = -\frac{a}{3}e^{-t/\tau} [\cos(\omega t) + \cos(2\omega t) + \cos(3\omega t)] + b, \quad (4)$$

where a, b, τ, ω are fitting parameters. Along with the STO data, we separately measure the total atom number N_{tot} in the lattice with no PA laser for dissipation. Similarly, we also measure the total atom number N in the lattice after the irradiation of the PA laser for dissipation. We quantify the magnetic correlation by the normalized STO amplitude A and the number of singlet pairs N_s and triplet pairs N_{t_0} , and their fractions $p_s = N_s/N_{\text{tot}}$ and $p_{t_0} = N_{t_0}/N_{\text{tot}}$:

$$A = 2a/N_{\text{tot}}, \quad (5)$$

$$p_s = N_s/N_{\text{tot}} = (N + a - b)/N_{\text{tot}}, \quad (6)$$

$$p_{t_0} = N_{t_0}/N_{\text{tot}} = (2N - 3a - 2b)/2N_{\text{tot}}. \quad (7)$$

In the derivation, we assume the SU(6) symmetry in the six-component mixture.

Dynamical reversal of the magnetic correlation in a double-well lattice.— To reveal the effects of the on-site two-body loss on the magnetic correlation, we first measure the spin correlation dynamics in a dissipative double-well lattice. Figures 2(a), 2(b) and 2(c) show the results of the normalized STO amplitude A , the singlet fraction p_s , and the triplet fraction p_{t_0} , respectively. The STO data are taken for the atom number $N_{\text{tot}} = 2.7 \times 10^4$, which is small enough to suppress double occupancies. Dimensionless dissipation strength $\gamma' = \gamma/U = \hbar(\gamma_{\text{PA}}/2)/U$ is 0.082(4), where γ_{PA} is the two-body loss rate due to the PA laser and is measured from atom loss dynamics in a double-well lattice (Sec. S.2 in SM [27]). In this measurement, the dependency of the spin correlation dynamics on the magnitude of initial ($t_{\text{PA}} = 0$) antiferromagnetic correlations is also investigated, which is realized by changing atom-loading schemes into a double-well lattice (Sec. S.3 in SM [27]). In Fig. 2(a), the normalized STO amplitude decreases as the dissipation is introduced, regardless of the initial conditions. Especially, in the initial condition (ii), the form of the STO signal reverses due to the

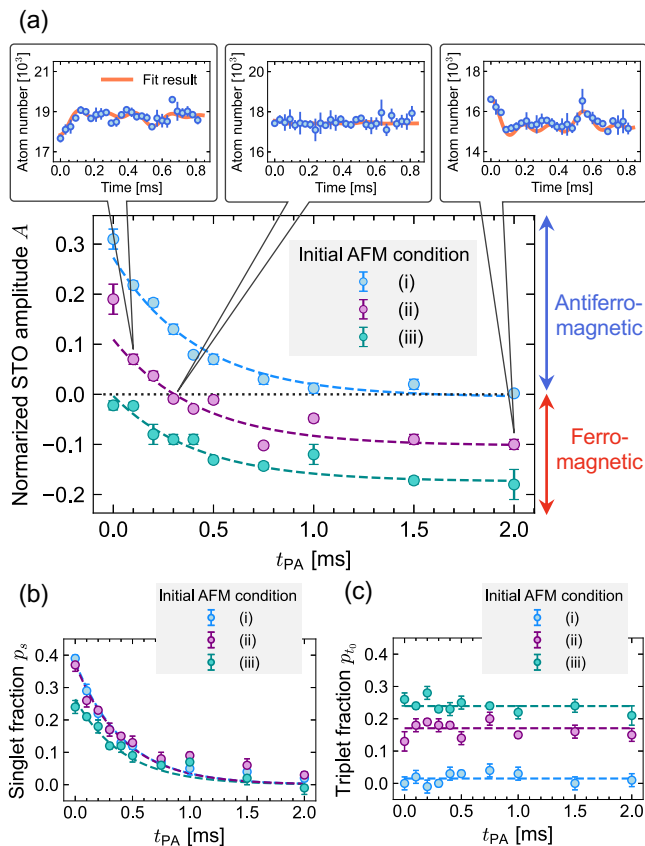


FIG. 2. Dynamics of (a) the normalized STO amplitude A , (b) the singlet fraction p_s , and (c) the triplet fraction p_{t_0} in a double-well lattice with on-site two-body losses. Here, we show the dependency of them on the irradiation time t_{PA} of the PA laser. In (a), three different initial antiferromagnetic (AFM) conditions are prepared with different atom-loading schemes into an optical lattice (Sec. S.3 in SM [27]). The dashed curves in (a), (b) and (c) show the results of the exponential fit with an offset, without an offset, and the constant fit, respectively, where the damping time constant of the exponential function is determined by the co-fit to A and p_s . Error bars denote the standard deviation, which is calculated with fitting errors of STO measurement and the standard deviations of the total atom number. In markup balloons in (a) (upper), measured STO signals for the initial condition (ii) are shown, which correspond to $t_{PA} = 0.1$ ms, 0.3 ms and 2.0 ms in order from the left. Error bars in STO signals denote the standard deviation of three scans.

dissipation, indicating the sign of A changing from positive to negative (Fig. 2: upper left to right). This means that the magnetic correlation between the nearest neighbor sites in the double-well lattice changes from an antiferromagnetic to ferromagnetic correlation, which has been theoretically predicted [15] and corresponds to the negative spin temperature state [23] (Sec. S.4 in SM [27]). Note that the photon scattering by the PA laser, which can decrease spin correlations, is negligible on the time scale of this measurement. Figure 2(b) shows that the singlet fraction p_s decreases by the

application of the dissipation, while the triplet fraction p_{t_0} shows no apparent decrease, as shown in Fig. 2(c). These results are in good agreement with the theoretical consideration that the change of the spin correlation is solely due to the decrease of the number of the singlet state while that of the triplet state is kept constant.

Dependency of the dissipative dynamics on dissipation strength and exchange interaction.— Next, we investigate the dependency of the spin correlation dynamics in a double-well lattice on the dissipation strength γ' and the exchange interaction $J = 4t_d^2/U$. When $U \gg t_d$, the loss rate Γ of the singlet state is theoretically given as $\Gamma = J\gamma'/(1 + \gamma'^2)$ [15]. Considering $\gamma' \ll 1$ for this measurement, we expect the linear dependency of the decay rate of p_s on γ' and J . Figure 3(a) (left) shows the result of the singlet fraction p_s measured at each dissipation strength γ' . One can clearly see that the larger the dissipation strength is, the faster p_s decays. In Fig. 3(a) (right), we show the dependency of the decay rate of p_s on the dissipation strength γ' . We find that the decay rate of p_s increases approximately in proportion to γ' . The dotted line in Fig. 3(a) (right) shows the result of the calculation considering the finite value of $U/t_d = 4$ in our case, which is consistent with the data (see Sec. S.5 in SM [27] for the details of the calculation). Figure 3(b) (left) shows the result of the singlet fraction p_s measured at each short lattice depth, where the dissipation strength is fixed at $\gamma' = 0.082(4)$. The shallower the short lattice depth is, namely, the larger the magnitude of the exchange interaction J is, the faster p_s decays. We note that U/t_d changes from 4.0 to 10.9 when $s_{\text{short}}^{(z)}$ changes from 5.2 to 8.0. In Fig. 3(b) (right), we show the dependency of decay rate of p_s on the exchange interaction J . We find that the decay rate of p_s increases approximately in proportion to J (see S.5 in SM [27] for the dependency of the calculated loss rate of the singlet state on J considering the finite value of U/t_d in our case).

Crossover from a double-well lattice to a 1D uniform lattice.— Finally, we measure spin correlations in the presence of the dissipation in a crossover from a double-well lattice to a 1D uniform lattice. Figure 4(a) shows the result of the dependency of the normalized STO amplitude A on the long lattice depth. Here, we prepare a sample with a small antiferromagnetic correlation in the absence of the dissipation (Sec. S.3 in SM [27]). In this measurement, the dissipation strength γ' is fixed to 0.082(4). We note that we restrict the irradiation time of the PA laser t_{PA} to 0.5 ms in this measurement to suppress the effect of hopping between 1D tubes and photon scattering by the PA laser. As shown in Fig. 4(a), we find that the formation of the ferromagnetic spin correlation is suppressed for the smaller long-lattice depths at which atoms can tunnel to neighboring double wells during the irradiation time of the PA laser $t_{PA} = 0.5$ ms. The quantity $2t_{PA}t/\hbar$ is

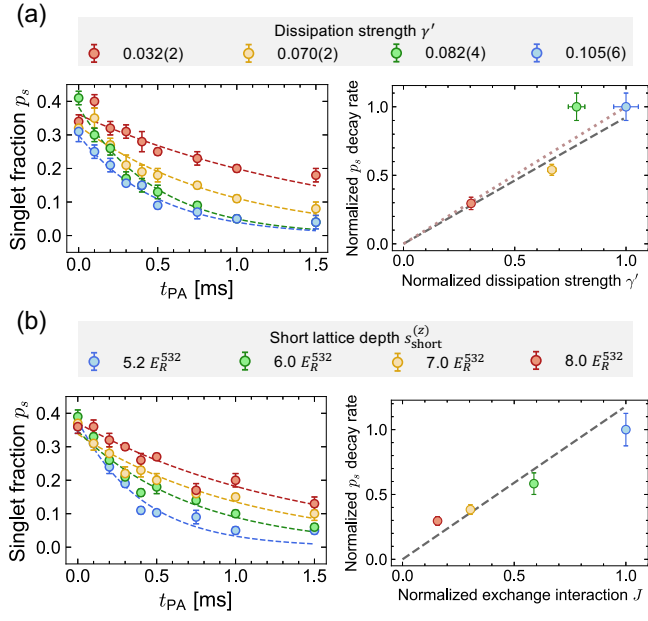


FIG. 3. (a) (left) Dynamics of the singlet fraction p_s for each dissipation strength γ' in a dissipative double-well lattice. Each dashed curve shows the results of the exponential fit without an offset. (right) Dependency of the decay rate of p_s obtained by the exponential fit on the dissipation strength γ' . The black dashed line shows the result of the linear fit through the origin. The dotted line shows the result of the calculation considering the finite value of $U/t_d = 4$ in our case. Here, the value of each axis is normalized by its maximum value. Vertical error bars denote the fitting error of the exponential fit to p_s . Horizontal error bars denote the errors of the measured two-body loss rates. (b) (left) Dynamics of the singlet fraction p_s for each short lattice depth in a dissipative double-well lattice. Here, E_R^{532} denotes the recoil energy of the short lattice. Each dashed line shows the results of the exponential fit without an offset. (right) Dependency of the decay rate of p_s obtained by the exponential fit on the exchange interaction J . The black dashed line shows the result of the linear fit through the origin. Here, the value of each axis is normalized by its maximum value.

a measure of such a probability, which is plotted as the red solid curve in Fig. 4(a), and the black dashed line represents the value of 1. It can be qualitatively understood that this suppression is due to the combined effect of on-site two-body losses and holes created by tunneling between double wells. The previous work [15] has also pointed out that numerically calculated spin correlations between nearest-neighbor sites of a 1D uniform lattice are smaller than those of a double-well lattice. Special emphasis is given to the result for the 1D uniform lattice ($s_{long}^{(z)} = 0$), where A is small but definitely nonzero and negative. In Fig. 4(b), we show the STO signal for a 1D uniform lattice. These results clearly indicate that in the 1D uniform lattice, the magnetic correlation also reverses, and the ferromagnetic correlation emerges. For all lattice configurations dealt with in this measurement,

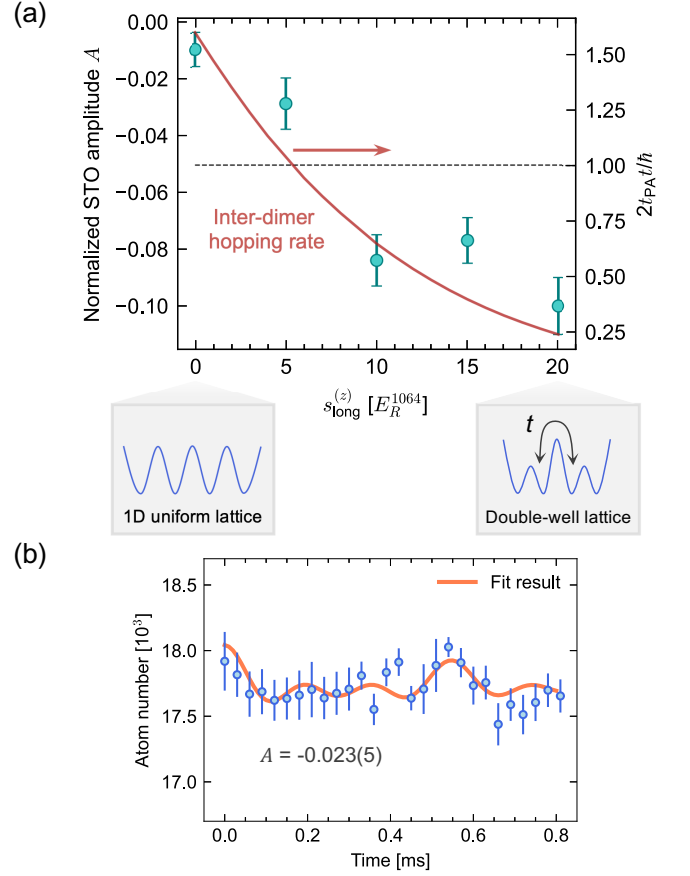


FIG. 4. (a) Normalized STO amplitude A in a crossover from a double-well lattice to a 1D uniform lattice. Here, the dependency of A on the long lattice depth is shown. We note that the number of scans in STO measurement at $0 E_R^{1064}$ is seventeen, otherwise three. The red solid curve shows the tunneling rate $2t_{PA}t/\hbar$ between double wells (right axis), which is normalized by the irradiation time of the PA laser $t_{PA} = 0.5$ ms, and the black dashed line represents the value of 1. Here, the factor 2 corresponds to tunnelings to double wells on both sides. (b) Measured STO signal in a 1D uniform lattice of $s_L = (100, 80, 8, 0)$. The orange solid curve shows the fit result. Error bars denote the standard error of twelve scans.

the steady state is expected to be the Dicke state. However, steady states are considered unachieved in this measurement as the right axis in Fig. 4(a) shows that the irradiation time of the PA laser is comparable with the inter-dimer hopping time, which is the consequence of the restriction of the irradiation time of the PA laser for the reasons mentioned above. So far, in a dissipative 1D uniform lattice, the formation of the Dicke state, which has a fully symmetric spin wave function and shows a the ferromagnetic correlation, has only been indirectly suggested based on the atom loss dynamics [19]. The observed ferromagnetic correlation in this work provides a more direct signature of the transient state leading to the steady Dicke state.

Summary and outlook.— We have systematically

investigated the effects of dissipation on the quantum magnetism in a double-well lattice and a 1D uniform lattice. We have observed the dynamical reversal of the magnetic correlation as dissipation is introduced in a double-well lattice, and the reversed magnetic correlation is observed in a wide range of lattice configurations, which more directly suggests the formation of a transient ferromagnetic spin correlation leading to a highly entangled Dicke state.

As a future outlook, quantum gas microscope (QGM) is expected to directly observe the effect of the dissipation on the long-range magnetic correlation due to the spin-charge separation in a 1D uniform lattice and its dynamics [28, 29]. A QGM may also allow us to observe the dissipation-induced spin-charge separation in a 1D uniform lattice, which has been theoretically predicted [30]. In higher dimensions (2D and 3D), the spin-charge separation does not occur. Thus, the behavior of the long-range magnetic correlation in a dissipative 2D or 3D system is an interesting problem. Moreover, the reversal of the magnetic correlation is also predicted for a bosonic system [15]. By utilizing the 3P_2 state of ^{174}Yb , which has the spin degrees of freedom and intrinsic inelastic interaction between them [12], the reversal may be experimentally observed.

We acknowledge Masahito Ueda for helpful discussions. This work was supported by the Grant-in-Aid for Scientific Research of JSPS (Nos. JP17H06138, JP18H05405, JP18H05228, JP20K14383, JP21H01014), the Impulsing Paradigm Change through Disruptive Technologies (ImPACT) program, JST CREST (No. JP-MJCR1673), and MEXT Quantum Leap Flagship Program (MEXT Q-LEAP) Grant No. JP-MXS0118069021.

* honda.kantaro.35m@st.kyoto-u.ac.jp

- [1] A. J. Daley, Quantum trajectories and open many-body quantum systems, *Advances in Physics* **63**, 77 (2014).
- [2] M. Müller, S. Diehl, G. Pupillo, and P. Zoller, Engineered open systems and quantum simulations with atoms and ions, *Advances In Atomic, Molecular, and Optical Physics*, **61**, 1 (2012).
- [3] G. Barontini, R. Labouvie, F. Stubenrauch, A. Vogler, V. Guarrera, and H. Ott, Controlling the dynamics of an open many-body quantum system with localized dissipation, *Phys. Rev. Lett.* **110**, 035302 (2013).
- [4] R. Labouvie, B. Santra, S. Heun, S. Wimberger, and H. Ott, Negative differential conductivity in an interacting quantum gas, *Phys. Rev. Lett.* **115**, 050601 (2015).
- [5] R. Labouvie, B. Santra, S. Heun, and H. Ott, Bistability in a driven-dissipative superfluid, *Phys. Rev. Lett.* **116**, 235302 (2016).
- [6] A. Müllers, B. Santra, C. Baals, J. Jiang, J. Benary, R. Labouvie, D. A. Zezyulin, V. V. Konotop, and H. Ott, Coherent perfect absorption of nonlinear matter waves, *Science Advances* **4**, eaat6539 (2018).
- [7] Y. S. Patil, S. Chakram, and M. Vengalattore, Measurement-induced localization of an ultracold lattice gas, *Phys. Rev. Lett.* **115**, 140402 (2015).
- [8] H. P. Lüschen, P. Bordia, S. S. Hodgman, M. Schreiber, S. Sarkar, A. J. Daley, M. H. Fischer, E. Altman, I. Bloch, and U. Schneider, Signatures of many-body localization in a controlled open quantum system, *Phys. Rev. X* **7**, 011034 (2017).
- [9] N. Syassen, D. M. Bauer, M. Lettner, T. Volz, D. Dietze, J. J. García-Ripoll, J. I. Cirac, G. Rempe, and S. Dürr, Strong dissipation inhibits losses and induces correlations in cold molecular gases, *Science* **320**, 1329 (2008).
- [10] B. Yan, S. A. Moses, B. Gadway, J. P. Covey, K. R. A. Hazzard, A. M. Rey, D. S. Jin, and J. Ye, Observation of dipolar spin-exchange interactions with lattice-confined polar molecules, *Nature* **501**, 521 (2013).
- [11] T. Tomita, S. Nakajima, I. Danshita, Y. Takasu, and Y. Takahashi, Observation of the Mott insulator to superfluid crossover of a driven-dissipative Bose-Hubbard system, *Science Advances* **3**, e1701513 (2017).
- [12] T. Tomita, S. Nakajima, Y. Takasu, and Y. Takahashi, Dissipative Bose-Hubbard system with intrinsic two-body loss, *Phys. Rev. A* **99**, 031601 (2019).
- [13] M. J. Mark, E. Haller, K. Lauber, J. G. Danzl, A. Janisch, H. P. Büchler, A. J. Daley, and H.-C. Nägerl, Preparation and spectroscopy of a metastable Mott-insulator state with attractive interactions, *Phys. Rev. Lett.* **108**, 215302 (2012).
- [14] M. J. Mark, S. Flannigan, F. Meinert, J. P. D’Incao, A. J. Daley, and H.-C. Nägerl, Interplay between coherent and dissipative dynamics of bosonic doublons in an optical lattice, *Phys. Rev. Research* **2**, 043050 (2020).
- [15] M. Nakagawa, N. Tsuji, N. Kawakami, and M. Ueda, Dynamical sign reversal of magnetic correlations in dissipative Hubbard models, *Phys. Rev. Lett.* **124**, 147203 (2020).
- [16] R. H. Dicke, Coherence in spontaneous radiation processes, *Phys. Rev.* **93**, 99 (1954).
- [17] M. Foss-Feig, A. J. Daley, J. K. Thompson, and A. M. Rey, Steady-state many-body entanglement of hot reactive fermions, *Phys. Rev. Lett.* **109**, 230501 (2012).
- [18] A. B. Lorenzo Rosso, Leonardo Mazza, The eightfold way to dark states in $SU(3)$ cold gases with two-body losses (2022), arXiv:2201.12889 [cond-mat.quant-gas].
- [19] K. Sponselee, L. Freystatzky, B. Abeln, M. Diem, B. Hundt, A. Kochanek, T. Ponath, B. Santra, L. Mathey, K. Sengstock, and C. Becker, Dynamics of ultracold quantum gases in the dissipative Fermi-Hubbard model, *Quantum Science and Technology* **4**, 014002 (2018).
- [20] H. Ozawa, S. Taie, Y. Takasu, and Y. Takahashi, Antiferromagnetic spin correlation of $SU(N)$ Fermi gas in an optical superlattice, *Phys. Rev. Lett.* **121**, 225303 (2018).
- [21] S. Taie, E. Ibarra-García-Padilla, N. Nishizawa, Y. Takasu, Y. Kuno, H.-T. Wei, R. T. Scalettar, K. R. A. Hazzard, and Y. Takahashi, Observation of antiferromagnetic correlations in an ultracold $SU(N)$ Hubbard model (2020), arXiv:2010.07730 [cond-mat.quant-gas].
- [22] F. Görg, M. Messer, K. Sandholzer, G. Jotzu, R. Desbuquois, and T. Esslinger, Enhancement and sign change of magnetic correlations in a driven quantum many-body system, *Nature* **553**, 481 (2018).

- [23] N. F. Ramsey, Thermodynamics and statistical mechanics at negative absolute temperatures, *Phys. Rev.* **103**, 20 (1956).
- [24] D.-S. Lühmann, O. Jürgensen, M. Weinberg, J. Simonet, P. Soltan-Panahi, and K. Sengstock, Quantum phases in tunable state-dependent hexagonal optical lattices, *Phys. Rev. A* **90**, 013614 (2014).
- [25] S. Taie, R. Yamazaki, S. Sugawa, and Y. Takahashi, An SU(6) Mott insulator of an atomic Fermi gas realized by large-spin Pomeranchuk cooling, *Nature Physics* **8**, 825 (2012).
- [26] S. Trotzky, Y.-A. Chen, U. Schnorrberger, P. Cheinet, and I. Bloch, Controlling and detecting spin correlations of ultracold atoms in optical lattices, *Phys. Rev. Lett.* **105**, 265303 (2010).
- [27] See Supplemental Material at [URL will be inserted by publisher] for the experimental details and the calculation method which includes Refs. [1, 11, 20, 23, 31–35].
- [28] T. A. Hilker, G. Salomon, F. Grusdt, A. Omran, M. Boll, E. Demler, I. Bloch, and C. Gross, Revealing hidden antiferromagnetic correlations in doped Hubbard chains via string correlators, *Science* **357**, 484 (2017).
- [29] J. Vijayan, P. Sompert, G. Salomon, J. Koepsell, S. Hirthe, A. Bohrdt, F. Grusdt, I. Bloch, and C. Gross, Time-resolved observation of spin-charge deconfinement in fermionic Hubbard chains, *Science* **367**, 186 (2020).
- [30] M. Nakagawa, N. Kawakami, and M. Ueda, Exact liouvilian spectrum of a one-dimensional dissipative Hubbard model, *Phys. Rev. Lett.* **126**, 110404 (2021).
- [31] C. Haimberger, J. Kleinert, O. Dulieu, and N. P. Bigelow, Processes in the formation of ultracold NaCs, *Journal of Physics B* **39**, S957 (2006).
- [32] S. D. Kraft, M. Mudrich, M. U. Staudt, J. Lange, O. Dulieu, R. Wester, and M. Weidemüller, Saturation of Cs₂ photoassociation in an optical dipole trap, *Phys. Rev. A* **71**, 013417 (2005).
- [33] U. Schlöder, C. Silber, T. Deuschle, and C. Zimmermann, Saturation in heteronuclear photoassociation of ⁶Li⁷Li, *Phys. Rev. A* **66**, 061403 (2002).
- [34] M. Junker, D. Dries, C. Welford, J. Hitchcock, Y. P. Chen, and R. G. Hulet, Photoassociation of a Bose-Einstein condensate near a Feshbach resonance, *Phys. Rev. Lett.* **101**, 060406 (2008).
- [35] S. Braun, J. P. Ronzheimer, M. Schreiber, S. S. Hodgman, T. Rom, I. Bloch, and U. Schneider, Negative absolute temperature for motional degrees of freedom, *Science* **339**, 52 (2013).

Supplemental Material for Observation of the Sign Reversal of the Magnetic Correlation in a Driven-Dissipative Fermi-Hubbard System

S.1 SINGLET-TRIPLET OSCILLATION MEASUREMENT

The STO measurement is performed after the atom-loading to an optical lattice in 150 ms and the irradiation of the PA laser to induce dissipation. The specific sequence of the STO measurement is as follows (Fig. S1). Note that we call a probed dimer the specific neighboring sites for measuring the spin correlation.

(1) Tunneling freezing : we freeze tunneling between intra- and inter- dimer sites by ramping up the long lattice depth of double wells to $s_L = (80, 80, (20.8, 25))$ in 0.5 ms, followed by ramping up the short lattice depth to $s_L = (80, 80, (80, 25))$ in 10 ms. We note that the adiabaticity of this ramp up sequence is confirmed by numerical calculation (Supplemental Material of Ref. [S1]).

(2) STO : we drive STOs in probed dimers by irradiating a gradient beam, which induces a spin-dependent potential gradient on atoms. This potential gradient creates an energy difference Δ for atoms with different spins in a probed dimer, and the spin states in the dimer coherently oscillate between the singlet state $|s\rangle = (|\sigma_1, \sigma_2\rangle - |\sigma_1, \sigma_2\rangle)/\sqrt{2}$ and the triplet state $|t_0\rangle = (|\sigma_1, \sigma_2\rangle + |\sigma_1, \sigma_2\rangle)/\sqrt{2}$ at a frequency Δ/\hbar (STO frequency), where $\sigma_i (i = 1, 2)$ denotes a spin component. In this work, we use a linearly polarized light with 2.7 GHz blue detuning from the $^1S_0 \leftrightarrow ^3P_1$ ($F' = 7/2$) transition as the gradient beam, which makes STO frequencies the same for the spin pairs of ($|m_F| = 1/2, 3/2$) with the corresponding STO frequency ω_1 , ($3/2, 5/2$) with ω_2 , and ($1/2, 5/2$) with ω_3 . In addition to this, a simple relation $\omega_1 : \omega_2 : \omega_3 = 1 : 2 : 3$ holds between these frequencies due to the properties of the Clebsch-Gordan coefficients for the associated transition. Note that an STO does not occur for the spin pairs of $(-1/2, 1/2)$, $(-3/2, 3/2)$, and $(-5/2, 5/2)$. We also note that actually observed STO signals suffer from the decoherence mainly due to the spatial inhomogeneity of the gradient beam. This effect is taken into account in an exponential decay term in the fitting function (Eq. (4) in the main text).

(3) Site merging : we ramp down the short lattice depth to $s_L = (80, 80, (0, 25))$ in 1 ms. Here, two atoms in the singlet state which has a spatially symmetric two-particle wave function both occupy the lowest band, while for two atoms in the triplet state which has a spatially antisymmetric two-particle wave function, one atom occupies the lowest band and the other atom occupies the first excited band.

(4) Irradiation of the PA laser : we irradiate the PA laser and remove two atoms which doubly occupy the

lowest band, corresponding to the detection of the singlet states. The PA laser in the STO sequence is detuned by -812 MHz from the $^1S_0 \leftrightarrow ^3P_1$ ($F' = 7/2$) transition [S1, S2]. After irradiating the PA laser, the absorption imaging follows, in which observed atom number dynamics reflects the magnetic correlation of the prepared sample.

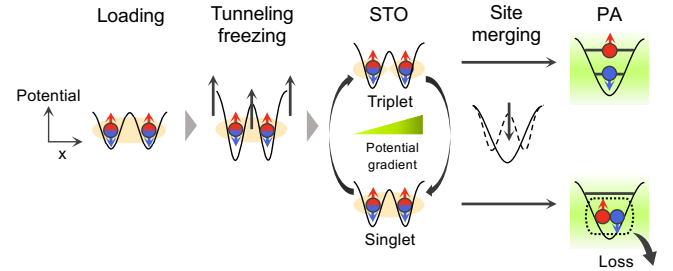


FIG. S1. Schematic illustration of the sequence for STO measurement in a dimer. Here, we show the case of two spins (red and blue) per dimer. The sequence flows as loading, tunneling freezing, STO, site merging and PA. Depending on the STO time, the two spins form the state in which one spin occupies the lowest band and the other spin occupies the first excited band, or the state in which both spins occupy the lowest band. Atoms in the latter state are removed by the PA.

S.2 LOSS RATE MEASUREMENT OF PA

To induce on-site two-body losses as dissipation, we apply the PA laser which is detuned by -5.76 GHz from the $^1S_0 \leftrightarrow ^3P_1$ ($F' = 7/2$) transition. We measure on-site two-body loss rate due to the PA laser in a double-well lattice of $s_L = (80, 80, (20.8, 20))$, into which evaporatively cooled six-component ^{173}Yb atoms are loaded. Here, unlike the spin correlation measurement, we load a sufficient number of atoms to prepare doubly occupied sites. In Fig. S2, we show the results of the loss rate measurement and a typically observed atom loss dynamics (inset). Here, we fit the data with a double exponential function where the initial faster decay corresponds to the on-site two-body loss and the later slower decay corresponds to the one-body loss mainly due to the photon-scattering. We note that we observe the saturation of loss rate γ_{PA} at a large intensity of the PA laser, which has also been observed in previous works [S3–S7], and we only use the PA intensities in the unsaturated regime. The PA light does not play a role in one-body losses or the heating effect since the photon-scattering rate for atoms of single occupation at intensity $\sim 20 \text{ W/cm}^2$ is calculated to be $\gamma_{\text{photon}} = 0.021 / \text{ms}$, which ensures that the effect

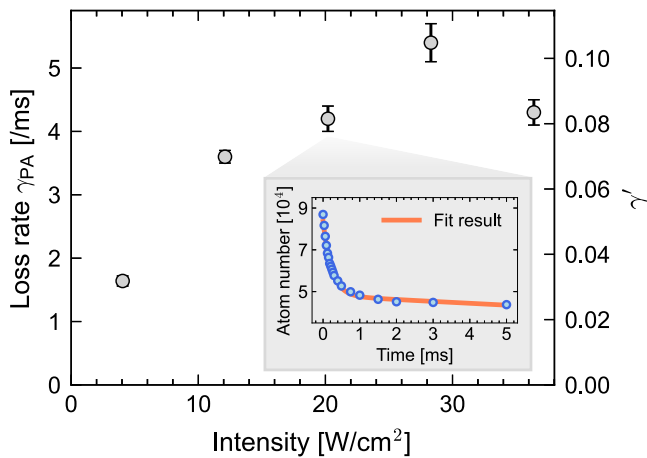


FIG. S2. Two-body loss rate γ_{PA} due to the PA laser. Here, we show the dependency of the loss rate γ_{PA} (dimensionless dissipation strength γ' in the right axis) on the intensity of the PA laser. Error bars denote the fitting error to the atom loss dynamics. The inset shows the typical observed atom loss dynamics, where the orange solid curve shows the fit result by a double exponential function. Error bars denote the standard deviation of three scans (smaller than the plots).

of photon scattering is negligible in the time scale that we measure the dynamics in this work (< 2 ms).

S.3 LOADING SCHEMES TO REALIZE THREE DIFFERENT INITIAL ANTIFERROMAGNETIC CONDITIONS

In the investigation of the dynamics in a dissipative double-well lattice, we prepare three systems with different initial antiferromagnetic (AFM) conditions (i), (ii), and (iii) in Fig. 2. These are realized by different atom-loading schemes to a double-well lattice. The specific sequence is as follows (Fig. S3):

- (i) Large AFM condition (normalized STO amplitude $A \sim 0.3$).
Load to double-well lattices along z -axis, which has a lattice depth of $s_L = (80, 80, (20.8, 20))$, from the beginning.
- (ii) Medium AFM condition ($A \sim 0.2$)
First load to a three-dimensional lattice and switch to double-well lattices along z -axis in 0.5 ms : $s_L = (28, 28, (28, 0)) \rightarrow (80, 80, (20.8, 20))$.
- (iii) Small AFM condition ($A \sim 0.0$)
First load to one-dimensional lattices along x -axis and switch to double-well lattices along z -axis in 0.5 ms : $s_L = (19.8, 80, (80, 0)) \rightarrow (80, 80, (20.8, 20))$.

In the measurement of spin correlations in the crossover from a double-well lattice to a uniform one-dimensional

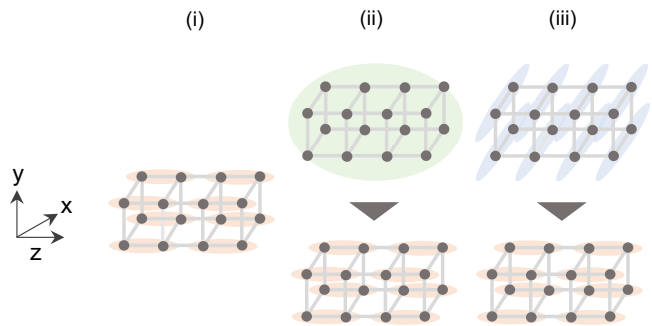


FIG. S3. Schematic illustration of three different atom-loading schemes into double-well lattices : (i) Load to double-well lattices along z -axis from the beginning. (ii) First load to a three-dimensional lattice and switch to double-well lattices along z -axis in 0.5 ms. (iii) First load to one-dimensional lattices along x -axis and switch to double-well lattices along z -axis in 0.5 ms.

lattice, we prepare systems with small initial AFM correlations by a loading scheme similar to (iii).

S.4 SPIN TEMPERATURE

In the state with sign-reversed magnetic correlations, the population of triplet states is greater than that of singlet states, which corresponds to a negative temperature state [S8]. Here, we define the spin temperature T_{spin} as

$$\frac{p_{t_0}}{p_s} = \exp\left(-\frac{J}{k_B T_{\text{spin}}}\right), \quad (\text{S1})$$

where k_B is the Boltzmann constant, p_s/p_{t_0} is the singlet/triplet fraction, and J is the exchange interaction. In Fig. S4, we show the result of the dynamics of $1/T_{\text{spin}}$ measured in a dissipative double-well lattice, which corresponds to the result for the initial AFM condition (ii) shown in Fig. 2. As dissipation is introduced, $1/T_{\text{spin}}$ reverses from positive to negative via positive infinity at which $p_s = p_{t_0}$. This result demonstrates that a negative temperature state, which has been realized in an isolated system [S9], can also be realized in an open quantum system with dissipation.

S.5 SINGLET LOSS RATE AT FINITE U/t_d

In the main text (Fig. 3), we investigate the singlet loss rate in a double-well lattice. To theoretically evaluate the singlet loss rate at finite U/t_d , we consider a two-site Fermi-Hubbard model with on-site two-body loss. The dynamics of the density matrix $\hat{\rho}$ of this system is described by the quantum master equation (Eq. (1) in the main text). Here, we use the quantum-trajectory method [S10], in which the system evolves under the effective non-

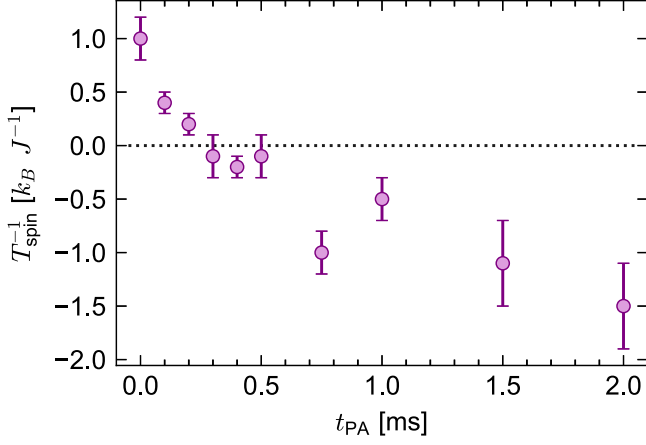


FIG. S4. Dynamics of the inverse of the spin temperature T_{spin} calculated from the result for the initial AFM condition (ii) shown in Fig. 2(b) and 2(c). Here, we show the dependency of the inverse of T_{spin} on the irradiation time t_{PA} of the PA laser. Error bars denote the standard deviation, which is calculated from the standard deviations of p_s and p_{t_0} .

Hermitian Hamiltonian

$$\begin{aligned} \hat{H}_{\text{eff}} &= \hat{H} - \frac{i}{4} \sum_j \sum_{\sigma \neq \sigma'} \hat{L}_{j\sigma\sigma'}^\dagger \hat{L}_{j\sigma\sigma'} \\ &= -t_d \sum_{\sigma} \left(\hat{c}_{1\sigma}^\dagger \hat{c}_{2\sigma} + \text{H.c.} \right) + \frac{\tilde{U}}{2} \sum_{j=1,2} \sum_{\sigma \neq \sigma'} \hat{n}_{j\sigma} \hat{n}_{j\sigma'} \end{aligned} \quad (\text{S2})$$

during a time interval between loss events. The imaginary part of the complex-valued interaction strength $\tilde{U} := U - i\gamma$ is due to the inelastic interaction that causes on-site two-body loss [S11]. If the system has two particles with spin σ_1 and σ_2 ($\sigma_1 \neq \sigma_2$), the eigenvalues E_n and the corresponding right eigenstates $|n\rangle_R$ of the non-Hermitian Hamiltonian (S2) are given by

$$E_0 = \frac{1}{2}(\tilde{U} - \sqrt{\tilde{U}^2 + 16t_d^2}), \quad (\text{S3})$$

$$|0\rangle_R = -\frac{2t_d}{E_0}(|\sigma_1, \sigma_2\rangle - |\sigma_2, \sigma_1\rangle) + |0, \sigma_1\sigma_2\rangle + |\sigma_1\sigma_2, 0\rangle, \quad (\text{S4})$$

$$E_1 = 0, \quad (\text{S5})$$

$$|1\rangle_R = |\sigma_1, \sigma_2\rangle + |\sigma_2, \sigma_1\rangle, \quad (\text{S6})$$

$$E_2 = \tilde{U}, \quad (\text{S7})$$

$$|2\rangle_R = |0, \sigma_1\sigma_2\rangle - |\sigma_1\sigma_2, 0\rangle, \quad (\text{S8})$$

$$E_3 = \frac{1}{2}(\tilde{U} + \sqrt{\tilde{U}^2 + 16t_d^2}), \quad (\text{S9})$$

$$|3\rangle_R = -\frac{2t_d}{E_3}(|\sigma_1, \sigma_2\rangle - |\sigma_2, \sigma_1\rangle) + |0, \sigma_1\sigma_2\rangle + |\sigma_1\sigma_2, 0\rangle, \quad (\text{S10})$$

where

$$|\sigma_1, \sigma_2\rangle = \hat{c}_{1\sigma_1}^\dagger \hat{c}_{2\sigma_2}^\dagger |\text{vac}\rangle,$$

$$|\sigma_2, \sigma_1\rangle = \hat{c}_{1\sigma_2}^\dagger \hat{c}_{2\sigma_1}^\dagger |\text{vac}\rangle,$$

$$|\sigma_1\sigma_2, 0\rangle = \hat{c}_{1\sigma_1}^\dagger \hat{c}_{1\sigma_2}^\dagger |\text{vac}\rangle,$$

$$|0, \sigma_1\sigma_2\rangle = \hat{c}_{2\sigma_1}^\dagger \hat{c}_{2\sigma_2}^\dagger |\text{vac}\rangle,$$

and $|\text{vac}\rangle$ denotes the vacuum state. Note that these eigenstates are not normalized. We also note that the left eigenstates $|n\rangle_L$ are obtained by replacing \tilde{U} in $|n\rangle_R$ by \tilde{U}^* , and we thus have $|1\rangle_L = |1\rangle_R$ and $|2\rangle_L = |2\rangle_R$.

Using the non-Hermitian Hamiltonian, we consider the time evolution of the ground state of \hat{H} , i.e., the singlet state

$$\begin{aligned} |\psi(0)\rangle &= \frac{1}{\mathcal{N}} \left[\frac{4t_d}{-U + \sqrt{U^2 + 16t_d^2}} (|\sigma_1, \sigma_2\rangle - |\sigma_2, \sigma_1\rangle) \right. \\ &\quad \left. + |0, \sigma_1\sigma_2\rangle + |\sigma_1\sigma_2, 0\rangle \right], \end{aligned} \quad (\text{S11})$$

where \mathcal{N} is a normalization factor that ensures $\langle\psi(0)|\psi(0)\rangle = 1$. In the dynamics under \hat{H}_{eff} , the squared norm of a state is not conserved due to non-Hermiticity. The squared norm, which is initially normalized to unity, corresponds to the probability of having no loss events during the dynamics [S10]. Thus, the decay rate of the squared norm of the singlet state (S11) corresponds to the decay rate of the singlet fraction p_s . Using the completeness relation $\sum_n |n\rangle_R \langle n|_L \langle n|_R = 1$, we can write the time evolution of the squared norm of the solution of the Schrödinger equation $i\hbar d|\psi(t)\rangle/dt = \hat{H}_{\text{eff}}|\psi(t)\rangle$ as

$$\begin{aligned} \langle\psi(t)|\psi(t)\rangle &= \sum_{m,n} c_{m,n} e^{i(E_m^* - E_n)t/\hbar} \\ &= c_{0,0} e^{2\text{Im}[E_0]t/\hbar} + c_{3,3} e^{2\text{Im}[E_3]t/\hbar} \\ &\quad + c_{0,3} e^{i(E_0^* - E_3)t/\hbar} + c_{3,0} e^{i(E_3^* - E_0)t/\hbar}, \end{aligned} \quad (\text{S12})$$

where

$$c_{m,n} := \frac{\langle\psi(0)|m\rangle_L \langle n|\psi(0)\rangle_R}{\langle m|m\rangle_L \langle n|n\rangle_R} \langle m|n\rangle_R, \quad (\text{S13})$$

and we have used $\langle 1|\psi(0)\rangle = \langle 2|\psi(0)\rangle = 0$ in the second line of Eq. (S12). For the parameters used in our experiment, we find $|c_{3,3}|, |c_{0,3}|, |c_{3,0}| \ll c_{0,0}$ and $c_{0,0} \simeq 1$. Thus, the time evolution of the squared norm is approximated as

$$\langle\psi(t)|\psi(t)\rangle \simeq e^{-2\Gamma t/\hbar}, \quad (\text{S14})$$

and the singlet decay rate is given by 2Γ with

$$\begin{aligned} \Gamma &= -\text{Im}[E_0] \\ &= \frac{1}{2} \left(\gamma - \sqrt{\frac{-x + \sqrt{x^2 + y^2}}{2}} \right), \end{aligned} \quad (\text{S15})$$

where $x := U^2 + 16t_d^2 - \gamma^2$ and $y := -2U\gamma$.

In the main text, we find that the decay rate of p_s increases approximately in proportion to the exchange interaction $J = 4t_d^2/U$. Such a linear dependence is expected for $U \gg t_d$, whereas U/t_d takes a value be-

tween 4.0 and 10.9 in our case. We confirm that Γ is approximately proportional to J under the fixed dimensionless dissipation strength $\gamma' = \gamma/U$ even in the regime of $U \gtrsim t_d$. In Fig. S5, we show the dependence of

$$\frac{\Gamma}{\gamma'J} = \frac{1}{8} \left(\frac{U}{t_d}\right)^2 - \frac{1}{8\gamma'} \left(\frac{U}{t_d}\right)^2 \sqrt{\frac{-1 - 16(t_d/U)^2 + (\gamma')^2 + \sqrt{(1 + 16(t_d/U)^2 - (\gamma')^2)^2 + 4(\gamma')^2}}{2}} \quad (\text{S16})$$

on the short-lattice depth $s_{\text{short}}^{(z)}$. The dependency of $\Gamma/(\gamma'J)$ on $s_{\text{short}}^{(z)}$ is small (deviation/mean < 21%), meaning that the plots of the singlet decay rate p_s against J fall approximately on the same line.

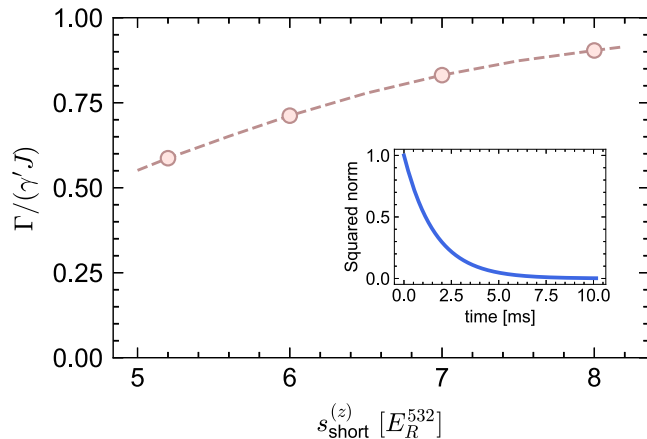


FIG. S5. Dependency of $\Gamma/(\gamma'J)$ on the short-lattice depth. Here, Γ is half of the singlet decay rate calculated with Eq. (S15), $\gamma' = \gamma/U$ is the dimensionless dissipation strength fixed to 0.082(4), and $J = 4t_d^2/U$ is the exchange interaction. The dots correspond to the values for $s_{\text{short}}^{(z)} = 5.2, 6.0, 7.0, 8.0$. The inset shows a typical result for the dynamics of the squared norm of the singlet state (S11) under \hat{H}_{eff} calculated with exact diagonalization for the parameters $U/t_d = 4.0$ and $\gamma' = 0.082$.

- SU(\mathcal{N}) Fermi gas in an optical superlattice, Phys. Rev. Lett. **121**, 225303 (2018).
- [S2] S. Taie, E. Ibarra-García-Padilla, N. Nishizawa, Y. Takasu, Y. Kuno, H.-T. Wei, R. T. Scalettar, K. R. A. Hazzard, and Y. Takahashi, Observation of antiferromagnetic correlations in an ultracold SU(N) Hubbard model (2020), arXiv:2010.07730 [cond-mat.quant-gas].
- [S3] T. Tomita, S. Nakajima, I. Danshita, Y. Takasu, and Y. Takahashi, Observation of the Mott insulator to superfluid crossover of a driven-dissipative Bose-Hubbard system, Science Advances **3**, e1701513 (2017).
- [S4] U. Schlöder, C. Silber, T. Deuschle, and C. Zimmermann, Saturation in heteronuclear photoassociation of $^6\text{Li}^7\text{Li}$, Phys. Rev. A **66**, 061403 (2002).
- [S5] S. D. Kraft, M. Mudrich, M. U. Staudt, J. Lange, O. Dulieu, R. Wester, and M. Weidemüller, Saturation of Cs_2 photoassociation in an optical dipole trap, Phys. Rev. A **71**, 013417 (2005).
- [S6] C. Haimberger, J. Kleinert, O. Dulieu, and N. P. Bigelow, Processes in the formation of ultracold NaCs, Journal of Physics B **39**, S957 (2006).
- [S7] M. Junker, D. Dries, C. Welford, J. Hitchcock, Y. P. Chen, and R. G. Hulet, Photoassociation of a Bose-Einstein condensate near a Feshbach resonance, Phys. Rev. Lett. **101**, 060406 (2008).
- [S8] N. F. Ramsey, Thermodynamics and statistical mechanics at negative absolute temperatures, Phys. Rev. **103**, 20 (1956).
- [S9] S. Braun, J. P. Ronzheimer, M. Schreiber, S. S. Hodgman, T. Rom, I. Bloch, and U. Schneider, Negative absolute temperature for motional degrees of freedom, Science **339**, 52 (2013).
- [S10] A. J. Daley, Quantum trajectories and open many-body quantum systems, Advances in Physics **63**, 77 (2014).
- [S11] M. Nakagawa, N. Tsuji, N. Kawakami, and M. Ueda, Dynamical sign reversal of magnetic correlations in dissipative Hubbard models, Phys. Rev. Lett. **124**, 147203 (2020).

[S1] H. Ozawa, S. Taie, Y. Takasu, and Y. Takahashi, Antiferromagnetic spin correlation of